# Effect of the grain size on hysteresis of liquid-crystalline Blue Phase I

**Prasenjit Nayek**
**Heon Jeong**
**Shin-Woong Kang**
**Seung Hee Lee** (SID Fellow)
**Heung-Shik Park**
**Hyuck Jin Lee**
**Hee Seop Kim**
**Gi-Dong Lee**

***Abstract*** — Three different blue-phase I liquid-crystal samples with different grain-size distribution were studied. Polycrystalline platelet grains reflects light in the visible region and have been observed under a polarizing optical microscope. Green and blue grain areas have been measured and then the statistical histogram by the Gaussian distribution function was fitted and the mean grain size was calculated. The effect of hysteresis on grain size has been compared for the three samples. Hysteresis depends explicitly on the grain-size distribution. Large grain size has revealed less hysteresis, while small grain size depicted pronounced hysteresis.

***Keywords*** — *Blue-phase liquid crystal, grain size, Kerr effect.*

DOI # 10.1889/JSID20.6.318

## 1 Introduction

Among the many types of mesophases, blue-phase (BP) liquid crystal has been studied due to their unique thermodynamical and structural properties,[1] phase sequences,[2–4] photonic applications,[5–8] and, of course, promising, next-generation high-frame-rate moving-image display device applications.[9–14] It has intermediate states that combine long-range positional or orientational order along some directions of space and liquid-like order along at least one of the other directions. Typically, blue phase arises due to high chirality and between the cholesteric phase and the isotropic phase. Among three types of stable BPs, two of these blue phases, BP I and BP II, exhibit cubic symmetry in which the orientational order is periodic and long range in three dimensions.[15] The third blue phase, referred to as BP III, has amorphous structure and symmetry as that of the isotropic phase.[16] The blue-phase structures involve a twist of the director (average molecular orientation) extending not only in one direction, such as in the cholesteric phase, but in both directions perpendicular to the director, referred to as double twist. This double twist cannot perfectly extend in three-dimensional space. Geometrical models of BPI and BPII consist of cubic networks of double-twist cylinders, separated by defect lines. The crystallographic space-group symmetries have been used to describe the long-range orientional order in the blue phase. The BP I director field possesses the symmetry group $O^8$ ($I4_132$) and BP II $O^2$ ($P4_232$).[15]

BP has many interesting properties which could be helpful to construct more realistic moving image quality with unprecedented image-driving speed. A fast submillisecond[17] order response time minimizes the motion-image blur and enables field-sequential-color displays without color filters if an RGB-LED backlight is used. The elimination of the color filters enhances optical efficiency by ~3×, resulting in lower power consumption if the same display brightness is compared and improves the device resolution as well as production cost. Wide viewing angle (thickness independent nature) and alignment layer less device application are also advantageous for high image quality and low cost. Although Kikuchi *et al.*[18] reported that the polymer-stabilized BP (PSBP) achieves a wide BP temperature range, but there are also some disadvantages. The operation voltage is too high (~50 $V_{rms}$) with respect to typical nematic LCDs (~5 $V_{rms}$). The transmittance of BPLCDs is relatively lower than that of nematic LCDs. In 2008, Samsung Electronics demonstrated a 15-in. BP LCD panel at Display Week for the first time.[13] Video image quality has been driven at 120 Hz, but the new technology will effectively double that to 240 Hz. This indicates that it could be exploited for in the fabrication of next-generation high-speed video reproduction. They use a protruded electrode[19] to reduce the operating voltage. The problem of high driving voltage and hysteresis is one of the major disadvantages of its commercialization. Hysteresis is an important parameter for BPLC as it affects the accuracy of gray-scale control. Hysteresis is not affected by polymer concentration but depends on the host liquid crystal and chiral dopants.[20] The influence of polymerization on temperature has also been reported by Fan *et al.*[21] In our recent paper,[22] we have demonstrated completely distinct switching routes, determined by the frequency of the electric field applied; however, the characteristic is associated with ionic mobility.

In this paper, we have concentrated on the effect of grain size of the polycrystalline BP I liquid crystal on the hysteresis. Here, we will address the hysteresis as well as operating voltage for three different BP-I samples which have different grain-size distribution. It is worthy to mention that BP I exhibits a higher transmittance and lower

P. Nayek, H. Jeong, S-W. Kang, and S. H. Lee are with Chonbuk National University, Department of BIN Fusion Technology and the Department of Polymer Nano Science and Technology, Deokjinku, Deokjindong 1Ga 664-14, Jeonju, Jeonbuk 561-756, Korea; telephone +82-63-270-2343, e-mail: lsh@chonbuk.ac.kr.
H-S. Park, H. J. Lee, and H. S. Kim are with the LCD Research Center, LCD Division, Samsung Electronics, Gyeonggi-do, Korea.
G-D. Lee is with Dong-A University, Department of Electronics Engineering, Pusan, Korea.

operating voltage, but inevitably it exhibits hysteresis.[23] We have chosen three different samples because they have almost the same Kerr constant and visible multidomain platelet structures. The results were compared in the BPI phase for all the three samples.

## 2 Materials parameters, cell structure, and fabricating process

The first BP sample, designated as LCMS-BP-081009-1, has the host nematic liquid-crystal mixture of cyanobiphenyl and cyanoterphenyl groups. The dielectric anisotropy ($\Delta\varepsilon$) = +14–17, and birefringence ($\delta n$) = 0.25–0.28, mixed with two chiral dopants, ZLI-4572 (8 wt.%) and CB15 (22 wt.%). The reflective range is within the visible region. The mixture (LC Matter Corporation, USA) showed the following phase sequence: Iso–65°C–BP–60°C– N*.The second sample, designated as LCMS-BP-11B (LC Matter Corporation, USA), has a host LC formulated from fluorinated biphenyl and cyanoester compounds. The dielectric anisotropy, $\Delta\varepsilon$ = + 57, and birefringence, $\delta n$ = 0.20, is mixed with chiral dopant, ZLI-4572 (13 wt.%). It exhibits the following phase sequence: Iso–58.7°C–BP–55.7°C 50N*. The third sample was designated as LCMS-BP-11A. It was formulated from fluorinated biphenyl and cyanoester LC host compounds. When the host LC, which has a dielectric anisotropy, $\Delta\varepsilon$ = + 48, and birefringence, $\delta n$ = 0.19, mixed with chiral dopant, ZLI-4572 (11 wt.%) flourished the following phase sequence: Iso–68.1°C–BP–64.5°C 50N*. Other information regarding mixtures are LC matter proprietary.

The LC mixture was sandwiched between two glass substrates. The upper glass substrate was plain glass, and the lower substrate was coated with patterned indium–tin oxide (ITO) electrodes with in-plane-switching (IPS) geometry. The cell parameters were as follows: an electrode width of 4 μm, electrode spacing of 4 μm, and cell gap ($d$) of 10 μm. For texture observation, the BPLC mixture was sandwiched between two glass substrates. The LC cells were observed inside the hot stage. The textures were taken by using an optical polarizing microscope (POM) Nikon DXM1200, which was interfaced with a digital camera via a computer. The temperature was controlled by a Linkam-TMS 94 model, and the cooling rate was 0.1°C/min. Before taking a reading, all the samples were stabilized at the BP-I temperature. For the electro-optic measurements we used He–Ne laser light with a wavelength, $\lambda$ = 633 nm. The cell was placed between a polarizer (towards the laser source) and an analyzer (towards the detector). The analyzer and polarizer were crossed to each other. In an IPS cell, the electric-field-induced birefringence takes place in the lateral direction. We rotated the cell azimuthally so that transmission is maximum in the voltage-on state. A digital oscilloscope, DPO 2012 from Tektronix, was used to measure the voltage-dependent–transmission ($V$–$T$) curve. The IPS device was driven with a variable-amplitude square-wave pulse (root mean square) at a frequency of 1 kHz from a function generator (Tektronix, AFG3022) connected to an amplifier. Finally, the intensity of the transmitted light is detected by a photodetector (Nanotek NLS-OP01). The transmittance was normalized by the maximum transmission. The voltage-holding ratio (VHR) was measured by using the VHR measurement system, VHR-200 (Sesim Photonics Technology, Korea). The measuring pulse width, frame frequency, and driving voltage was 1.0 msec, 60 Hz, and 10 V, respectively. The dielectric permittivity measurement has been performed by an Agilent 4284A precision LCR meter (20–1000 kHz). We observed the platelets textures and calculated the grain area by using Image-J software. Then, the area distribution of the grains was plotted in the form of a statistical histogram. We fitted the statistical histogram by using a Gaussian distribution function:

$$\mathbf{y} = y_0 + \frac{A}{w\sqrt{\pi/2}} e^{-2\frac{(x-x_c)^2}{w^2}}, \qquad (1)$$

where $y_0$ is the offset, $x_c$ is the mean (location of the peak), $w$ is the width, and $A$ is the area of the curve.

**TABLE 1** — The threshold voltage at 10% of the maximum transmission voltage, $V_{th}$ [$T_{10}$], and operating voltage, *i.e.,* the voltage at 90% of the maximum transmission, $V_{op}$ [$T_{90}$], is listed for three different BP I samples with different grain size.

| Parameter/Sample → ↓ | LCMS-BP-081009-1 | LCMS-BP- 11B | LCMS-BP- 11A |
|---|---|---|---|
| $V_{th}[T_{10}]$ (V) | 16 | 22 | 25 |
| $V_{op}[T_{90}]$ (V) | 54 | 57 | 60 |

## 3 Experimental results and discussion

Green and blue platelet grains for the sample LCMS-BP-081009-1 are shown in Fig. 1(a). Textural observations have been made at 62°C, *i.e.,* in the BP-I phase. Figure 1(b) shows the area distribution of the green-colored grains and Fig. 1(c) is the same for blue-colored grains. After fitting the statistical distribution by using Eq. (1), it revealed that the peak of the area distribution for green and blue grains are 3803 and 2879 $\mu m^2$, respectively. So, if we approximate the platelet grains as a square, then their length would be 62 and 54 μm for the green and blue grains, respectively. The $V$–$T$ curve for the sample LCMS-BP-081009-1 is represented in Fig. 2(a). The measured hysteresis ($\Delta V_{50}$) of the sample is ~4.8 $V_{rms}$. We defined the hysteresis by the voltage difference at 50% of the transmission level ($\Delta V_{50}$ , it is also the conventional method to define hysteresis for the BP ample).

A general question is why does hysteresis arise in the BPI phase? According to Coles[24] and Gleeson,[25] electric-field addressing causes local molecular reorientations and restoration of the BP-I structure. The structural restoration process in BP-I also affects the $V$–$T$ curves. Normally, transmittance is lower in the ramp-up voltage compared to the ramp-down voltage. The mechanisms are explained as fol-

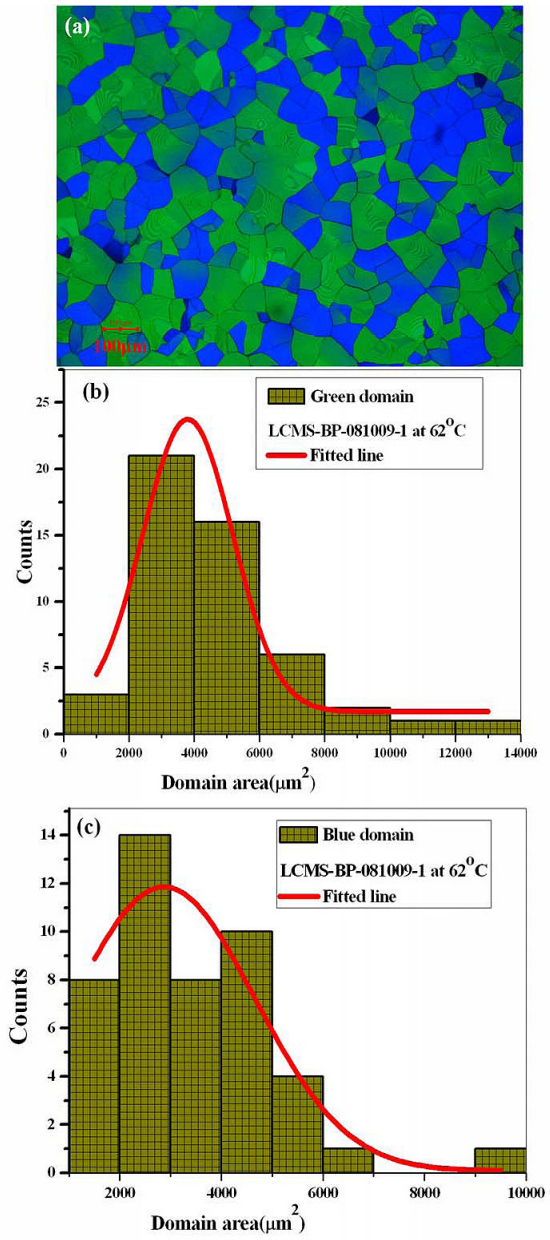


**FIGURE 1** — (a) POM texture for sample LCMS-BP-081009-1 shows the platelet grains of the green and blue color, (b) area distribution of the green-colored grains (statistical histogram) made from the above texture and the mean grain size is 62 μm, and (c) the statistical histogram for the blue-colored grains and mean grain size is 54 μm. The red line is the fitted Gaussian distribution function.

lows. As the voltage increases, the compact body-centered cubic packing of BP I prevents the LCs from unwinding, so that the induced birefringence is smaller, which leads to a lower transmittance.[23] Due to the compact packing, it also hinders the formation of the BP I structure during the voltage-descending process, which in turn leads to a higher transmittance when compared at the same voltage. As a result, the hysteresis loop is originated. So, compact packing is one of the main causes of the origin of hysteresis. In our experiment, the three different grain-sized samples have different hysteresis. It was observed that the longer the grain size, the lower the hysteresis effect. So, the small-grain-sized sample has the largest hysteresis due to its compact packing, whereas the largest-grain-sized sample has the smallest hysteresis due to flexible packing which is helpful in realizing a hysteresis-less display. In Fig. 2(a), the *V–T* curve shows higher transmission during forward voltage ramping. Due to less-compact packing and more-flexible structure of the large-sized grains, LCs could be easily unwound so that the induced birefringence is higher, which in turn leads to higher transmission for a ramp-up-voltage. On the other hand, during ramp-down voltage, a less-compact structure does not hinder the formation of the BPI structure, rather, it helps to return to its initial state, but large grain size slightly modified the defect and/or disclination lines in such a way that it has a small birefringence, and, as a result less transmission occurs. Further, we have calculated the operating voltage at 90% of the maximum transmission position, $V_{op}$ [$T_{90}$] = 54 V, whereas $V_{th}$ [$T_{10}$] = 16 V. It was found that the operating voltage and threshold voltage also depends on the grain size. They have a trade-off relationship with grain size. The electro-optical properties of the BP sample can be readily explained by the Kerr effect,[26] expressed as

$$\delta n = \lambda K E^2, \tag{2}$$

where $\delta n$, $\lambda$, and $E$ are the electric-field-induced birefringence, the wavelength of the incident light (633 nm in our case for a He–Ne laser) and the strength of the electric field, respectively. $K$ is the Kerr constant, which is entirely dependent on the material characteristics, indicating the magnitude of the Kerr effect and also is inversely proportional to the square of the operating voltage. Large-$K$ material typically plays an important role in lowering the operating voltage. Equation (2) is appropriate for small-electric-field approximation; otherwise, it diverges as $E$ increases. To determine the saturation trend of the experimental data, the following exponential convergence model proposed by Yan *et al.*[27] known as the extended Kerr effect, has been applied to derive the value of the Kerr constant as follows:

$$\delta n = \delta n_{sat}\left(1 - \exp\left[-\left(E/E_s\right)^2\right]\right), \tag{3}$$

where $\delta n_{sat}$ is the saturated refractive-index change and $E_s$ represents the saturation field. Interestingly, from a power-series expansion on Eq. (3), the $E^2$ term is obtained; *i.e.*, the Kerr effect under a small-electric-field approximation, and then the Kerr constant can be expressed as follows:

$$K = 3\delta n_{sat}/\lambda E_s^2. \tag{4}$$

We have extracted the Kerr constant by fitting the $\delta n$ *vs.* $E^2$ graph to the extended Kerr equation, *i.e.*, Eq. (3) and then substituting the values of $\delta n_{sat}$ and $E_S{}^2$ into Eq. (4). Figure 2(b) shows the experimental result (circle) and the fitted curve (line). Calculated $K$ is 1.25 nm/V$^2$. From our experiment on LCMS-BP-081009-1 BP, we have found that although its chiral concentration is higher than that of the

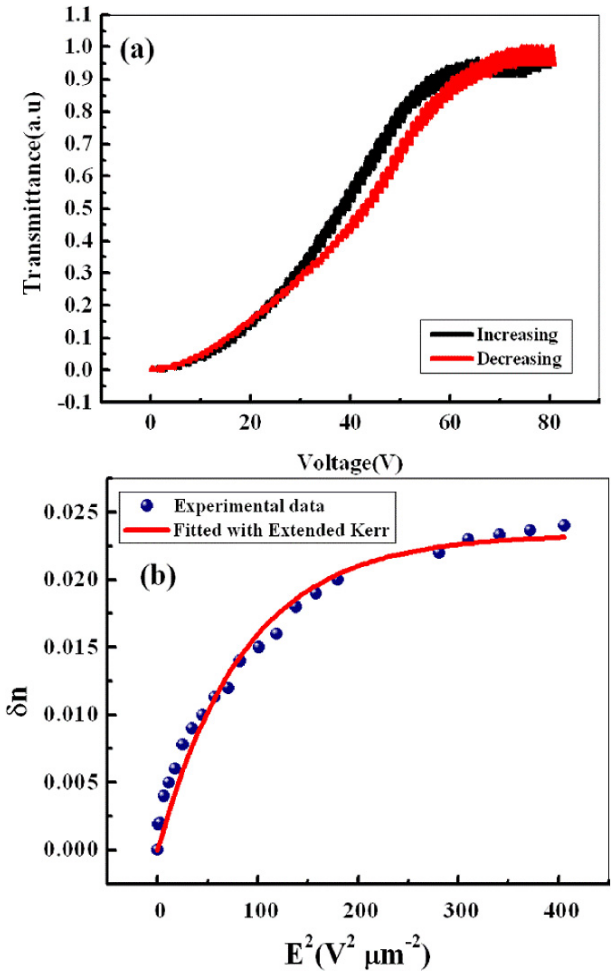


**FIGURE 2** — (a) Transmission *vs.* voltage (*V–T*) curve for the LCMS-BP-081009-1 sample, from this *V–T* curve, we measured the hysteresis, $\Delta V_{50} \sim 4.8 V_{rms}$, $V_{op}$ [$T_{90}$] = 54 V, and $V_{th}$ [$T_{10}$] = 16 V, and (b) experimentally determined induced birefringence *vs.* the square of the applied-electric-field graph and fitted (red line) curve with an extended Kerr-effect model. The calculated value of the Kerr constant from this graph is ~1.25 nm/V$^2$.

remaining two samples, we found that its Kerr constant is the largest. It is also clear that its maximum $\Delta\varepsilon \times \delta n$ product is 4.76, which is the smallest but the Kerr constant is the highest. So, from that we can conclude that *K* depends on the grain size. The larger the grain size, the greater the Kerr constant.

Similarly, Fig. 3(a) shows the texture of the platelet grains for the sample LCMS-BP-11B. Figures 3(b) and 3(c) shows the measured area distribution of the grains for green and blue grain colors. It revealed that grain size is about 26 and 27 μm for the green and blue grains, respectively. The textural observations were performed at 57°C, *i.e.*, in the BP-I phase. We have extracted from the *V–T* graph that the hysteresis ($\Delta V_{50}$) is ~7.9 V for this sample. LCMS-BP-11B has a smaller grain size compared to that of LCMS-BP-081009-1, so it has a larger hysteresis. One important point here, which should be addressed carefully, is that during voltage-ramp-up transmission the hysteresis is less and during ramp-down transmission is higher. This is just the opposite in the first case, *i.e.*, for the LCMS-BP-081009-1 sample. LCMS-BP-11B has a smaller grain size than LCMS-BP-081009-1. Due to its smaller grain size, it has a more-compact structure. When the voltage increases, this compact structure of BP I prevents the LCs from unwinding, so the induced birefringence is smaller which leads to a lower transmittance. Due to compact packing, it also hinders the formation of the BP I structure during the voltage-descending process, which, in turn, leads to a higher transmittance when compared at the same voltage. Like-

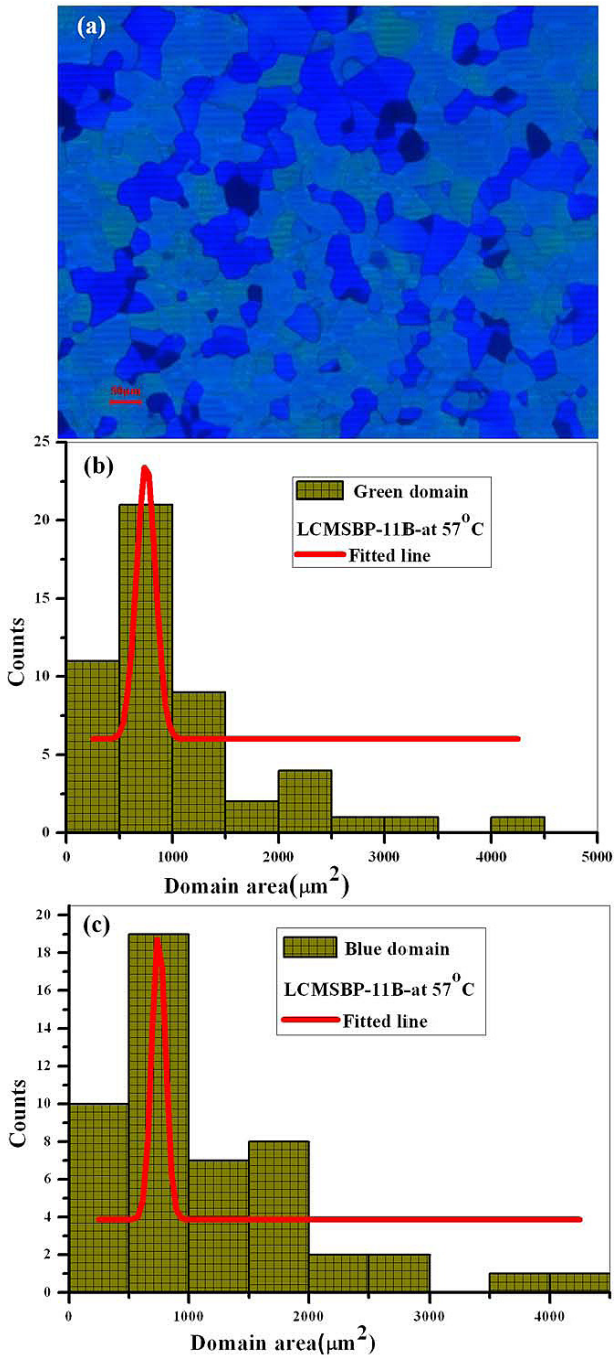


**FIGURE 3** — (a) POM texture for the LCMS-BP-11B sample, (b) area distribution of the green-colored grains made from the above texture and the mean grain size is 26 μm, and (c) statistical histogram for the blue-colored grains of mean size 27 μm. The red line is the fitted Gaussian distribution function.

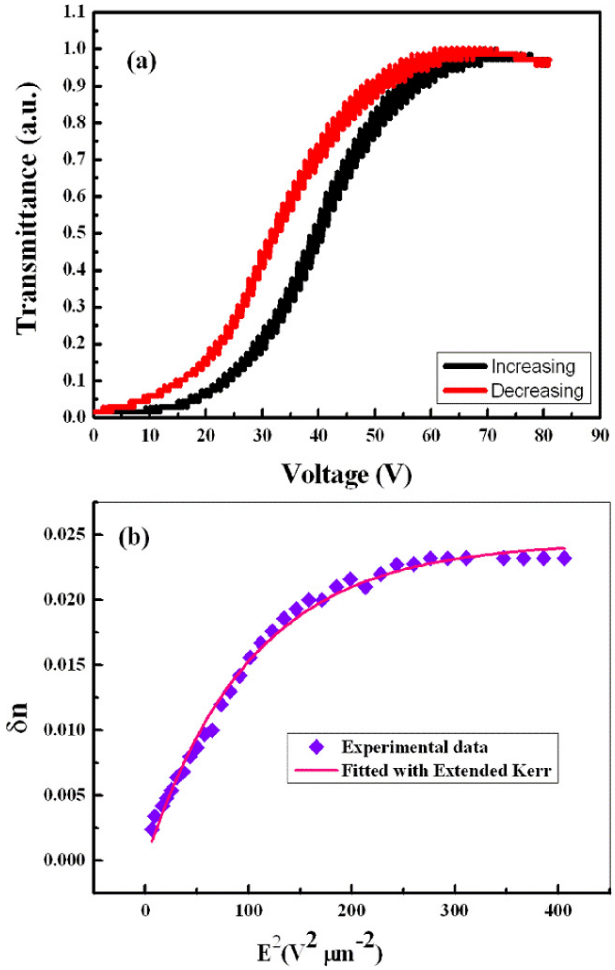


**FIGURE 4** — (a) *V–T* curve for the LCMS-BP-11B sample, the measured hysteresis is $\Delta V_{50} \sim 7.9 V_{rms}$, $V_{op}$ [$T_{90}$] = 57 V, and $V_{th}$ [$T_{10}$]= 22 V, and (b) induced birefringence *vs.* square of the applied-electric-field graph and fitted (red line) curve with an extended Kerr-effect model. The calculated value of the Kerr constant from this graph is ~1.13 nm/V$^2$.

wise, Fig. 4(a) depicts the *V–T* plot for the LCMS-BP-11B, and the calculated operating voltage and threshold voltages are $V_{op}$ [$T_{90}$] = 57 V, whereas $V_{th}$ [$T_{10}$] = 22 V. Calculated *K* for this case is 1.13 nm/V$^2$, and the fitted curve is shown in Fig. 4(b). Interestingly, Fig. 5(a) shows the texture of the platelet grains for the LCMS-BP-11A sample. Figures 5(b) and 5(c) show the measured area of the grain-area distribution for the green and blue grains, respectively. It revealed that grain size is about 10 μm for both cases. The picture and textural observations have been made at 65.5°C, *i.e.*, in the BP-I phase. Figure 6(a) depicts the *V–T* curve for the LCMS-BP-11A sample. We obtained a hysteresis ($\Delta V_{50}$) of 14.6 V, the largest of the three samples. It is logical as pointed out earlier that the smaller the grain size, the larger the hysteresis. Because this sample has the smallest grain size, the number of unit cells per unit volume is highest and so the compactness is also the highest. So, due to this compact structure, its hysteresis is also the largest and the operating voltage, $V_{op}$ [$T_{90}$], is 60 V and the threshold voltage, $V_{th}$ [$T_{10}$], is 25 V. The calculated *K* = 1.11 nm/V$^2$, which also gives the indication for a smaller pitch length. The real part

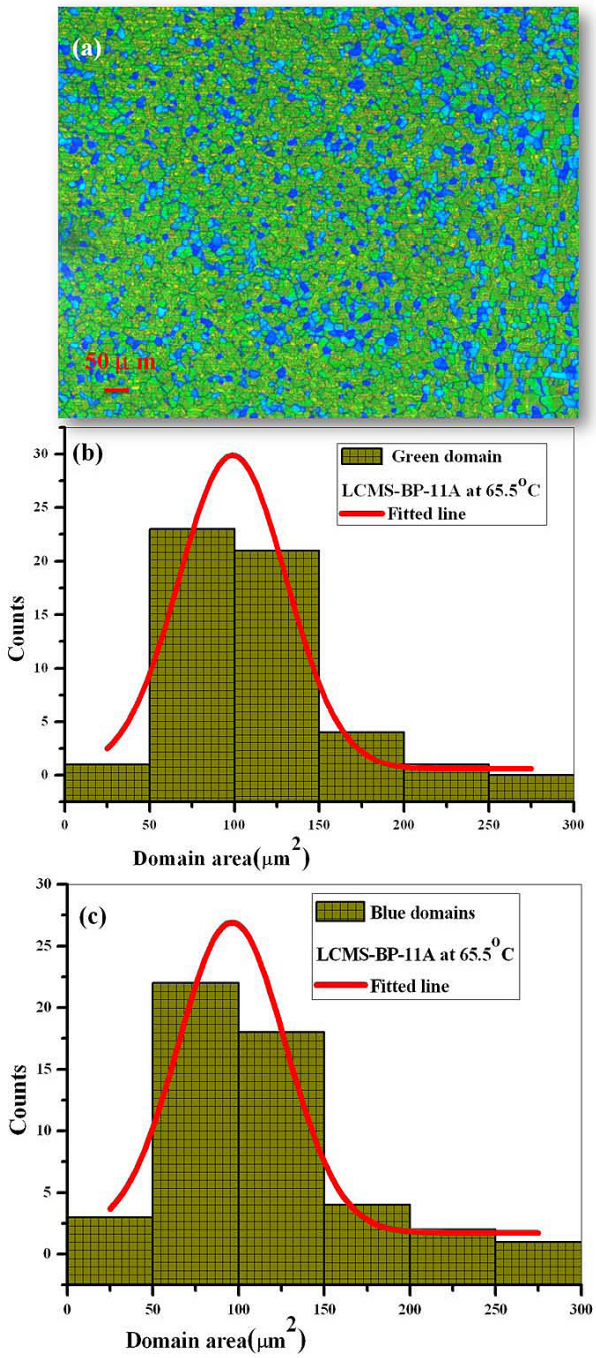


**FIGURE 5** — (a) POM texture for LCMS-BP-11A, (b) statistical histogram for the green-colored grains, and (c) statistical distribution for the blue-colored grains. The mean grain size for both cases are 10 μm. The red line is the fitted Gaussian distribution function.

of the dielectric permittivity is depicted in Fig. 7. For all the three samples, the low-frequency dielectric constant is almost same and also high with respect to the high-frequency dielectric constants. In general, low-frequency dielectric permittivity is related to dc conductivity or interfacial charges. So, we conclude that all three samples have almost the same residual charges, and it cannot affect the other parameters such as threshold voltage, operating voltage, and *K*. Nevertheless, for the 10–100 kHz region it is clear that the dielectric permittivity for LCMS-BP-11B

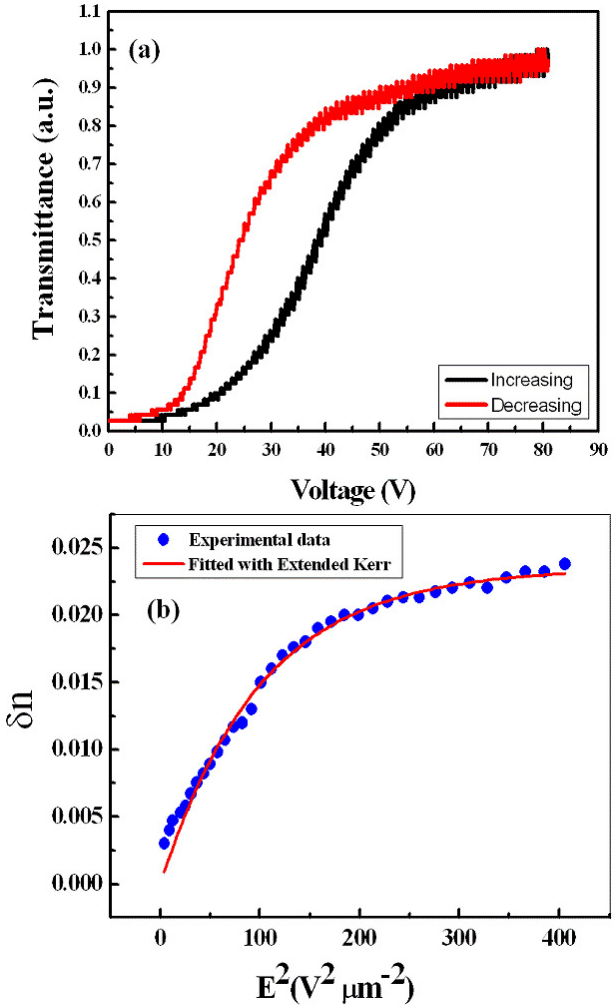


**FIGURE 6** — (a) *V–T* curve for the LCMS-BP-11A sample; from this *V–T* curve, the measured hysteresis was $\Delta V_{50}$ ~ 14.6 $V_{rms}$, $V_{op}$ [$T_{90}$] = 60 V, and $V_{th}$ [$T_{10}$] = 25 V, (b) experimentally determined induced birefringence *vs*. the square of the applied-electric-field graph and fitted (line) curve with an extended Kerr-effect model. The calculated value of the Kerr constant from this graph is ~1.11 nm/V$^2$.

($\Delta\varepsilon$ = + 57) is the highest, then LCMS-BP-11A ($\Delta\varepsilon$ = + 48), and finally LCMS-BP-081009-1 ($\Delta\varepsilon$ = +14–17) has lowest value which is mainly due to the decreasing order of the dielectric anisotropy of the materials.

The voltage-holding ratio is defined as the ratio of the RMS-voltage at a pixel within one frame period to the initial voltage value. We have measured the VHR by applying 10 V, in order to get an idea about the resistivity of each cell. We have found that VHR values for the three samples are almost same within 10%. This low value of VHR may be due to the use of high dielectric anisotropic material and chiral dopant which generates free-ion charges and reduces the VHR. Therefore, it could be inferred that the hysteresis and operating voltage of our results mainly depend on the grain size.

## 4 Summary

We can conclude that the large-grain-size BPI sample has less hysteresis which is helpful in display applications.

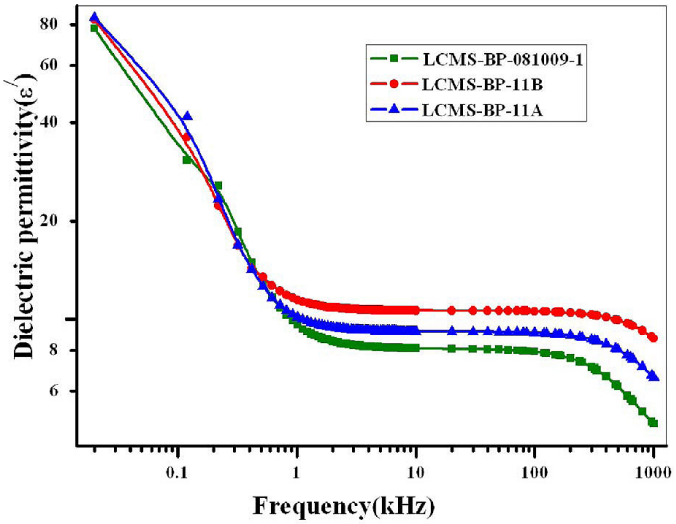


**FIGURE 7** — Shown is the real part of the dielectric permittivity with frequency. We have used a electrically controlled birefringence cell with a cell gap of 4 μm, and the strength of the probing signal was 1 V. In the frequency range of 10–100-kHz, it is clear that dielectric permittivity for LCMS-BP-11B ($\Delta\varepsilon$ ~ + 57) is highest, then LCMS-BP-11A ($\Delta\varepsilon$ ~ + 48), and finally LCMS-BP-081009-1 ($\Delta\varepsilon$ ~ + 14–17) has the lowest value which is mainly due to decreasing order of the dielectric anisotropy of the host materials.

Although we have demonstrated three samples with a maximum domain size of about 54–62 μm, it will be more interesting to see if the sample is monodomain. Therefore, the crystal structure and packing density play a dominant role in the hysteresis in the BPI sample. We are also expecting that if we can somehow synthesize monodomain BP that it will be more suitably exploited in display devices for their improved transmission and hysteresis. To ensure a concrete conclusion we are performing further experiments and will hopefully explore more details of these issues.

## Acknowledgment

This research was supported by the Basic Science Research Program through the National Research Foundation of Korea (2011-0003863) and also the WCU programme R31–20029 funded by the Ministry of Education, Science and Technology.

## References

1 H. Stegemeyer *et al.*, "Thermodynamic, structural and morphological studies on liquid-crystalline blue phases," *Liq. Cryst.* **1**, 3–28 (1986).
2 J. Rokunohe and A. Yoshizawa, "An unusual phase sequence of iso liq-blue phase-smectic A observed for novel binaphthyl mesogenic derivatives," *J. Mater. Chem.* **15**, 275–279 (2005).
3 M. H. Li *et al.*, "A chiral material with a new phase sequence: Twist grain boundary smectic A phase–blue phases," *Liq. Cryst.* **20**, 361–365(1996).
4 Z. Kutnjak *et al.*, "Supercritical conversion of the third blue phase to the isotropic phase in a highly chiral liquid crystal," *Phys. Rev. Lett.* **74**, 4859–4862 (1995).
5 W. Cao *et al.*, "Lasing in a three-dimensional photonic crystal of the liquid crystal blue phase II," *Nature Mater.* **1**, 111–113 (2002).
6 S. Yokoyama *et al.*, "Laser emission from a polymer-stabilized liquid-crystalline blue phase," *Adv. Mater.* **18**, 48–51 (2006).

7 Y.-H. Lin *et al.*, "Polarizer-free and fast response microlens arrays using polymer-stabilized blue phase liquid crystals," *Appl. Phys. Lett.* **96**, 113505/1-3 (2010).
8 J. Yan *et al.*, "High-efficiency and fast-response tunable phase grating using a blue phase liquid crystal," *Opt. Lett.* **36**, 1404–1406 (2011).
9 M. Lee *et al.*, "Liquid crystalline blue phase I observed for a bent-core molecule and its electro-optical performance," *J. Mater. Chem.* **20**, 5813–5816 (2010).
10 H. J. Coles and M. N. Pivnenko, "Liquid crystal 'blue phases' with a wide temperature range," *Nature* **436**, 997–1000 (2005).
11 Z. Ge *et al.*, "Modeling of blue phase liquid crystal displays," *J. Disp. Technol.* **5**, 250–256 (2009).
12 Z. Ge *et al.*, "Electro-optics of polymer-stabilized blue phase liquid crystal displays," *Appl. Phys. Lett.* **94**, 101104/1-3 (2009).
13 H. Lee *et al.*, "The World's first blue phase liquid crystal display," *SID Symposium Digest* **42**, 121–124 (2011).
14 S. Yoon *et al.*, "Optimisation of electrode structure to improve the electro-optic characteristics of liquid crystal display based on the Kerr effect," *Liq. Cryst.* **37**, 201–208 (2010).
15 S. Meiboom *et al.*, "Lattice symmetry of the cholesteric blue phases," *Phy. Rev. A* **28**, 3553–3560 (1983).
16 O. Henrich *et al.*, "Structure of blue phase III of cholesteric liquid crystals," *Phy. Rev. Lett.* **106**, 107801/1-4 (2011).
17 Y. Chen *et al.*, "A microsecond-response polymer-stabilized blue phase liquid crystal," *Appl. Phys. Lett.* **99**, 201105/1-3 (2011).
18 H. Kikuchi *et al.*, "Polymer-stabilized liquid crystal blue phases," - *Nature Mater.* **1**, 64–68 (2002).
19 L. Rao *et al.*, "Low voltage blue-phase liquid crystal displays," *Appl. Phys. Lett.* **95**, 231101/1-3 (2009).
20 J. Yan and S-T Wu, "Polymer effect on the electro-optic properties of blue-phase liquid crystals," *J. Display Technol.* **7**, 490–493 (2011).
21 C.-Y. Fan *et al.*, "Influence of polymerization temperature on hysteresis and residual birefringence of polymer stabilized blue phase LCs," *J. Display Technol.* **7**, 615–618 (2011).
22 A. Mukherjee *et al.*, "Emergence of a novel optically isotropic transient state with low frequency in a blue phase liquid crystal mixture," *Liq. Cryst.* **39**, 231–237 (2012).
23 K.-M. Chen *et al.*, "Hysteresis effects in blue-phase liquid crystals," *J. Display Technol.* **6**, 318–322 (2010).
24 H. J. Coles and H. F. Gleeson, "Electric field induced phase transitions and colour switching in the blue phases of chiral nematic liquid crystals," *Mol. Cryst. Liq. Cryst.* **167**, 213–225 (1989).
25 H. F. Gleeson and H. J. Coles, "Dynamic properties of blue-phase mixtures," *Liq. Cryst.* **5**, 917–926 (1989).
26 P. Weinberger, "John Kerr and his effects found in 1877 and 1878," *Philos. Mag. Lett.* **88**, 897–907 (2008).
27 J. Yan *et al.*, "Extended Kerr effect of polymer-stabilized blue-phase liquid crystals," *Appl. Phys. Lett.* **96**, 071105/1–3(2010).
28 L. Rao *et al.*, "A large Kerr constant polymer-stabilized blue phase liquid crystal," *Appl. Phys. Lett.* **98**, 081109 (2011).
29 M. Wittek *et al.*, "New materials for polymer-stabilized blue phase," *SID Symposium Digest* **42**, 292–293 (2011).

**Prasenjit Nayek** received his Ph.D. degree from Jadavpur University, India, in 2010. At present, he is working as a post-doctoral research assistant in the Department of BIN Fusion Technology, Chonbuk National University, South Korea. His main research interest is blue-phase liquid-crystal displays and liquid-crystal nanocomposites.

**Heon Jeong** received his B.E. degree from the Department of Polymer-Nano Science and Technology at Chonbuk National University in 2010. At present, he is working on his M.S. degree in the Department of Polymer Nano-Science and Technology at the same university. His main research field is the improvement in the properties of blue-phase liquid crystal and the stretching of carbon nanotubes by applying electric fields.

**Shin-Woong Kang** received his M.S. degree in chemistry from the Korea Advanced Institute of Science and Technology. After receiving his M.S. degree, he worked for Samsung from 1992 to 1997 in the field of liquid-crystal displays. In 2003, he obtained his Ph.D. degree from the Chemical Physics Interdisciplinary Program and Liquid Crystal Institute of Kent State University. After receiving his Ph.D., he worked on various liquid crystals and their applications at Kent State University for 6 years as a post-doctoral research associate, senior research scientist, and adjunct professor. Currently, he is a member of the faculty of the Department of BIN Fusion Technology at Chonbuk National University in Korea. His research interests cover various aspects of liquid-crystalline materials and their applications.

**Seung Hee Lee** received his B.S. degree in physics from Chonbuk National University in 1989 and his Ph.D. degree from the Physics Department of Kent State University in 1994. In 1995, he joined the LCD Division of Hyundai Electronics (now called HYDIS). Since then, he has developed and commercialized new liquid-crystal devices, called the fringe-field-switching (FFS) mode. He was awarded "Kink of the Invention" twice at the company. In September of 2001, he became a professor at Chonbuk National University in Chonju, Korea. He was selected as a SID Fellow in 2008 and was a Research Professor at Chonbuk National University from 2008 to 2010.

**Heeseop Kim** is Vice-President at Samsung Electronics, Korea. He received his B.S. degree in physics from Seoul National University, Korea, in 1987. He received his M.S. and Ph.D. degrees in materials science and engineering from POSTECH, Korea, in 1993 and 1997, respectively. He joined Samsung Electronics in 2000. He is responsible for advanced liquid-crystal materials and display technology at the R&D center.

**Hyeokjin Lee** received his B.S. and M.S. degrees in chemistry from Korea University in 1992 and 1995, respectively. In 2005, he received his Ph.D. degree from the University of Florida, USA, in the field of electronic materials in material science and engineering. His research interest in display materials, including LCDs and OLEDs. Currently, he is a principal engineer in the research and development of new liquid-crystal mode and materials at Samsung Electronics.

**Heung-Shik Park** received his B.S. (1996) and M.S. (1998) degrees in chemistry from Korea University, Korea. In 2010, he received his Ph.D. degree in chemical physics from Kent State University, USA. He was a Research Associate at the Liquid Crystal Institute at Kent State University from 2010 to 2011. His scientific interests are in the areas of liquid crystals (electro-optic effects, surface phenomena, and lyotropic systems) and nanomaterials for optical applications. He is currently working on a new display mode that uses liquid crystals as a principal engineer at the R&D center of Samsung Electronics.

**Gi-Dong Lee** received his B.S., M.S., and Ph.D. degrees in electronics from Pusan National University, Pusan, Korea, in 1989, 1991, and 2000, respectively. From 1991 to 1997, he was a research member of the R&D center of Samsung Display Devices Co., Ltd. From 2001 to 2003, he was with Dr. Philips J. Bos at the Liquid Crystal Institute, Kent State University, as a research fellow. Since 2004, he has been with the Department of Electronics Engineering at Dong-A university.